Exciton Radiative Lifetimes in Two-Dimensional Transition Metal Dichalcogenides

Maurizia Palummo,[†] Marco Bernardi,[‡] and Jeffrey C. Grossman*[,§]

[†]Dipartimento di Fisica, Università di Roma Tor Vergata, and European Theoretical Spectroscopy Facility (ETSF), Via della Ricerca Scientifica 1, 00133 Roma, Italy
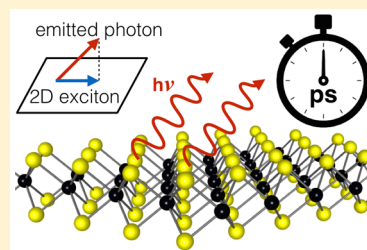
[‡]Department of Physics, University of California, Berkeley, California 94720, United States

[§]Department of Materials Science and Engineering, Massachusetts Institute of Technology, 77 Massachusetts Avenue, Cambridge, Massachusetts 02139-4307, United States

Ⓢ *Supporting Information*

ABSTRACT: Light emission in two-dimensional (2D) transition metal dichalcogenides (TMDs) changes significantly with the number of layers and stacking sequence. While the electronic structure and optical absorption are well understood in 2D-TMDs, much less is known about exciton dynamics and radiative recombination. Here, we show first-principles calculations of intrinsic exciton radiative lifetimes at low temperature (4 K) and room temperature (300 K) in TMD monolayers with the chemical formula MX_2 (X = Mo, W, and X = S, Se), as well as in bilayer and bulk MoS_2 and in two MX_2 heterobilayers. Our results elucidate the time scale and microscopic origin of light emission in TMDs. We find radiative lifetimes of a few picoseconds at low temperature and a few nanoseconds at room temperature in the monolayers and slower radiative recombination in bulk and bilayer than in monolayer MoS_2. The MoS_2/WS_2 and $MoSe_2/WSe_2$ heterobilayers exhibit very long-lived (~20−30 ns at room temperature) interlayer excitons constituted by electrons localized on the Mo-based and holes on the W-based monolayer. The wide radiative lifetime tunability, together with the ability shown here to predict radiative lifetimes from computations, hold unique potential to manipulate excitons in TMDs and their heterostructures for application in optoelectronics and solar energy conversion.

KEYWORDS: *Monolayer materials, transition metal dichalcogenides, luminescence, radiative lifetime, excitons, optoelectronics*

Two-dimensional (2D) transition metal dichalcogenides (TMDs) are promising materials for ultrathin electronic, optoelectronic, photocatalytic, and photovoltaic devices.[1−8] Out of approximately 40 existing TMDs,[9,10] some have received particular attention due to their semiconducting nature and tunable band gap. In particular, group 6 monolayer TMDs with chemical formula MX_2 (M = Mo, W and X = S, Se) are direct gap semiconductors with relatively intense photoluminescence (PL), while bilayers and thicker multilayers exhibit indirect gap and weaker PL.[1,10−17] The peculiar nature of the excited states has stimulated intense research efforts to investigate exciton dynamics and radiative/nonradiative lifetimes in TMDs.[13,18−24]

Recent time-resolved experiments found a range of characteristic times for exciton dynamics in monolayer TMDs, including fast (1−10 ps) recombination attributed to exciton trapping at defects, and slower processes on a 0.1−1 ns time scale interpreted as radiative exciton recombination.[18,20−22] However, the attribution of the observed signals to radiatiave and nonradiative processes can be ambiguous in time-resolved spectroscopies since defects and impurities can modulate the excited state dynamics. In TMDs, the interpretation of time signals and comparison among different experiments is further complicated by the use of micrometer-size flakes where the edges can play a significant role in exciton recombination. This situation has stimulated an ongoing quest for the intrinsic time

scale of exciton recombination in ideal, defect-free 2D-TMDs.[18,20−22] First-principles calculations combining density functional theory (DFT) and many-body perturbation theory are ideally suited to study excited state dynamics in layered 2D-TMDs.[25,26] These approaches can accurately predict excited state properties in the energy domain such as band gaps, exciton energies, and absorption/loss spectra,[26,27] and there is significant promise to extend these methods to study excited state processes in the time domain.[28−30]

In this work, we compute intrinsic exciton radiative lifetimes in layered 2D-TMDs from first principles. Our approach provides rich microscopic information about exciton recombination, yields radiative lifetimes in very good agreement with available experiments (without employing empirical fitting parameters), and elucidates the time scales observed in time-resolved experiments on 2D-TMDs. We demonstrate that the radiative lifetimes can be tuned over several orders of magnitude with number of layers, stacking sequence, and temperature, thus enabling unprecedented control of exciton dynamics in 2D-TMDs.

We combine DFT and the *GW*-Bethe Salpeter equation (BSE) method to compute the quasiparticle bandstructures, absorption spectra, and exciton energies and wavefunctions in 2D-TMDs. Our approach includes an accurate account of electron−electron, electron−hole, and spin−orbit interactions. The calculations are carried out using the Quantum Espresso and Yambo codes[31,32] (see Methods).

We employ Fermi's Golden rule to derive the radiative decay rate $\gamma_S(\mathbf{Q})$ of an exciton in state S with wavevector $\mathbf{Q}$ (and center-of-mass momentum $\hbar\mathbf{Q}$) in a 2D system

$$\gamma_S(\mathbf{Q}) = \tau_S^{-1}(\mathbf{Q}) = \gamma_S(0)\cdot\left\{\sqrt{1 - \left(\frac{\hbar c\, Q}{E_S(\mathbf{Q})}\right)^2} + \frac{1}{2}\frac{\left[\frac{\hbar c (Q_x - Q_y)}{E_S(\mathbf{Q})}\right]^2}{\sqrt{1 - \left(\frac{\hbar c\, Q}{E_S(\mathbf{Q})}\right)^2}}\right\} \tag{1}$$

where $Q = \|\mathbf{Q}\|$, Q_x and Q_y are the two in-plane wavevector components of the 2D exciton, $\tau_S(\mathbf{Q})$ is the radiative lifetime, defined here as the inverse of the decay rate, $E_S(\mathbf{Q})$ is the exciton energy, c is the speed of light, and $\gamma_S(0)$ is the decay rate for $\mathbf{Q} = 0$

$$\gamma_S(0) = \tau_S(0)^{-1} = \frac{8\pi e^2 E_S(0)}{\hbar^2 c}\frac{\mu_S^2}{A_{uc}} \tag{2}$$

with μ_S^2 as the square modulus of the BSE exciton transition dipole divided by the number of unit cells in 2D in the system (i.e., the number of 2D **k**-points employed in the calculation) and A_{uc} is the area of the unit cell. In eq 1, the first term in braces decreases from 1 for $Q = 0$ to zero for $Q = Q_0$ [where $Q_0 = E_S(Q_0)/\hbar c$], while the second term diverges for $Q = Q_0$; as shown in the Supporting Information, this divergence can be integrated and leads to a well-defined thermally averaged decay rate. Both terms in braces in eq 1 need to be set to zero for $Q > Q_0$ due to momentum conservation, so that the decay rate $\gamma_S(\mathbf{Q})$ vanishes for $Q > Q_0$. To compute the exciton radiative rate at temperature T, we average the rates up to the maximum momentum Q_0 using a parabolic exciton dispersion $E_S(\mathbf{Q}) = E_S(0) + [(\hbar^2 Q^2)/(2M_S)]$ (M_S is the exciton mass).[33] We obtain the average radiative lifetime $\langle\tau_S\rangle$ of an exciton in state S at temperature T

$$\langle\tau_S\rangle = \tau_S(0)\frac{3}{4}\left(\frac{E_S(0)^2}{2M_S c^2}\right)^{-1}k_B T \tag{3}$$

where the exciton energies and transition dipoles are obtained here from the BSE. The radiative lifetime in eq 3 increases linearly with temperature, similar to what has been found experimentally in 2D semiconductor quantum wells.[34,35] A detailed derivation of eqs 1−3 is discussed in the Supporting Information. At room temperature, we define an effective radiative lifetime $\langle\tau_{eff}\rangle$ obtained by further averaging the rates in eq 3 over the lowest-energy bright and dark excitons[33,36]

$$\langle\tau_{eff}\rangle^{-1} = \frac{\sum_S \langle\tau_S\rangle^{-1} e^{-E_S(0)/k_B T}}{\sum_S e^{-E_S(0)/k_B T}} \tag{4}$$

In this work, we employ eq 3 for the lifetime at low temperature and report the lifetimes obtained with both eq 3 and eq 4 at room temperature.

The electronic structure of group 6 TMD monolayers has been studied extensively.[10,11,13,15−17,37] The valence band maximum (VBM) and conduction band minimum (CBM)

are located at the **K** point of the Brillouin zone (BZ) and are mostly contributed by the *d* orbitals of the transition metal atoms.[9] The large spin−orbit coupling splits the VBM into two states with a well-defined spin projection, S_z, in the out-of-plane direction.[14] Because of lack of inversion symmetry in monolayer TMDs, there are two inequivalent **K** points in the BZ, called here $\mathbf{K}_\pm$. Time-reversal symmetry requires the VBM to be degenerate at $\mathbf{K}_\pm$ and the value of S_z at $\mathbf{K}_+$ to be opposite to the value at $\mathbf{K}_-$.[13,14]

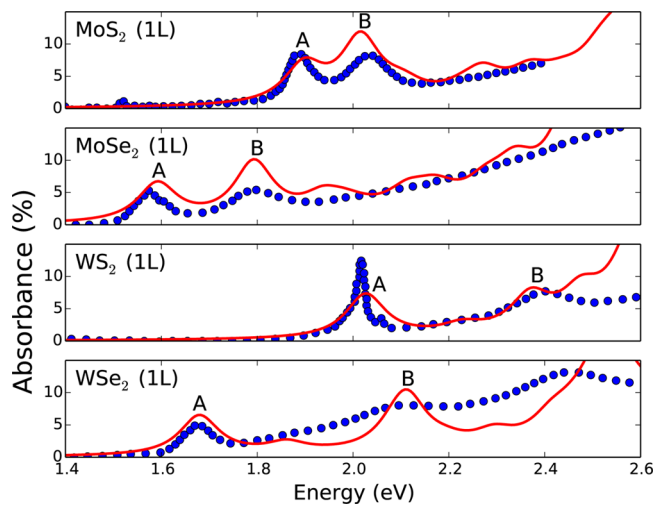Figure 1 shows the absorption spectra of the TMD monolayers studied here (the corresponding bandstructures

Figure 1. BSE (red line) and experimental (blue dots) absorption spectra of TMD monolayers. The experimental data are taken from ref 12 for MoS_2 and ref 24 for the other monolayers. The labels indicate the absorption peaks associated with the A and B excitons. The computed spectra were red-shifted by ~150 meV to match the experimental absorption onsets.

are shown in Figure S1 of the Supporting Information). Following a procedure from our recent work,[8] the BSE spectra are expressed in units of absorbance, here the percent fraction of absorbed light at each photon energy, thus enabling direct comparison with experiments. Our computed absorption onsets, defined here as the positions of the lowest-energy absorption peak, are in the 1.6−2.0 eV range and agree within ~150 meV with the experimental values measured at room temperature for all monolayers studied here. We attribute the small discrepancy to electron−phonon interactions decreasing the absorption onset at room temperature compared 0 K,[18,21] an effect not included in our calculations. The trends in the absorption spectra show very good agreement with experiments[12,24] and validate our BSE calculations employed below to obtain the radiative lifetimes. The two lowest-energy absorption peaks correspond to the so-called A and B excitons, respectively, and are associated with transitions at $\mathbf{K}_\pm$ from the two spin−orbit split VBM states to the CBM (see Figure 2a). The energies of the bright and dark excitons with A and B character are shown in Figure 2b. The bright and dark exciton character stems, respectively, from dipole-allowed and dipole-forbidden transitions at **K**. Because exciton thermalization occurs on a faster (~500 fs)[18,20] time scale than radiative recombination in monolayer TMDs, the radiative recombination of the bright A exciton is the main process contributing to PL.[12] In the W-based monolayers, we find a rich series of mostly dark excitons[38] at energies between the A and B peaks
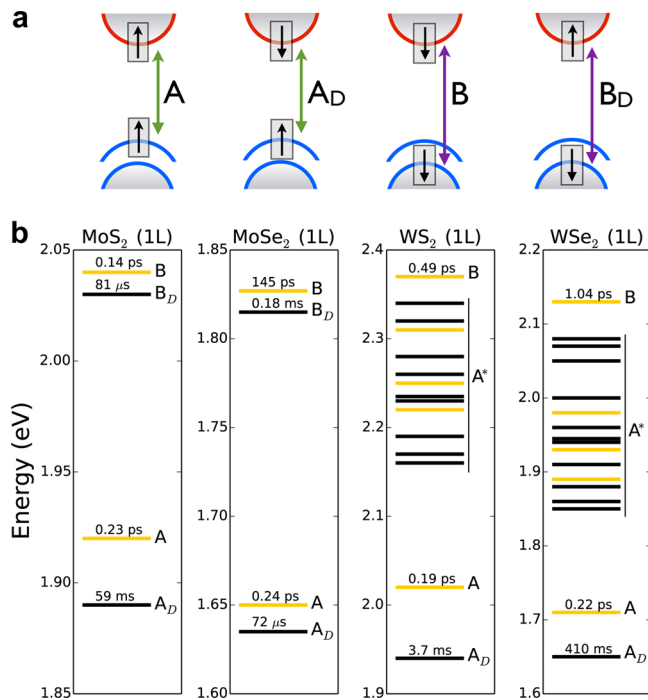
Table 1. Radiative Lifetimes in Monolayer TMDs[a]

		MoS$_2$	MoSe$_2$	WS$_2$	WSe$_2$
E_A	(eV)	1.9	1.65	2.0	1.7
$\tau_A(0)$	(ps)	0.23	0.24	0.19	0.22
$\langle \tau_A^{LT} \rangle$	(ps)	3.7	5.0	2.3	3.8
τ_{exp}^{LT}	(ps)	5[21] (S), 4.5[22] (S)			4[39] (S)
$\langle \tau_A^{RT} \rangle$	(ns)	0.27	0.38	0.17	0.29
$\langle \tau_{eff}^{RT} \rangle$	(ns)	0.82	0.80	4.4	3.5
τ_{exp}^{RT}	(ns)	0.85[18] (s)	0.9[40] (S)		4[41] (S)

[a]The data refers to the bright A exciton. E_A is the exciton energy, equal to the absorption onset. $\tau_A(0)$ is the computed radiative lifetime at 0 K. $\langle \tau_A^{LT} \rangle$ and $\langle \tau_A^{RT} \rangle$ are the computed radiative lifetimes at low temperature (4 K) and room temperature, respectively, and τ_{exp}^{LT} and τ_{exp}^{RT} are the corresponding experimental values. $\langle \tau_{eff}^{RT} \rangle$ is the room temperature effective lifetime computed by averaging the dark and bright rates (see eq 4). In the experimental data, (s) indicates a suspended layer, and (S) indicates a substrate-supported layer.

Figure 2. (a) Radiative processes associated with the A and B bright and dark (subscript D) excitons at the $\mathbf{K_+}$ point. The two spin−orbit split VBM states are shown in blue and the CBM in red. The processes at $\mathbf{K_-}$ (not shown) are the time-reversal of those shown here. (b) Energy and intrinsic radiative lifetime $\tau_S(0)$ at 0 K for the lowest-energy excitons in TMD monolayers. The dark and bright excitons are shown with black and yellow lines, respectively. The labels indicate the A, A∗, and B excitons.

(A∗ excitons in Figure 2b) made up by holes from the VBM and electrons from the CBM and the band above the CBM. The A∗ excitons are not expected to contribute significantly to PL in the W-based monolayers given that they are mostly dark and their energy difference with the A exciton is much larger than $k_B T$ at room temperature. Figure 2b shows the intrinsic radiative lifetimes $\tau_S(0)$ (see eq 2) of the lowest-energy excitons in monolayer TMDs, computed at 0 K and for excitons with zero momentum. These lifetimes are employed to obtain the thermally averaged radiative lifetimes of the bright A excitons at finite temperature, $\langle \tau_A \rangle$ (see eq 3).

The A exciton radiative lifetimes $\langle \tau_A \rangle$ at low temperature of 4 K and room temperature are the key quantities computed in this work and are shown in Table 1. We find lifetimes of 1−10 ps at 4 K and 1−5 ns at room temperature in the TMD monolayers studied here and predict a linear increase of the lifetimes between 0 K and room temperature at a rate of ∼1−10 ps/K. Because our radiative lifetimes are intrinsic and related to ideal and defect-free 2D-TMDs, they provide an important benchmark for time-resolved experiments.

We compare our computed radiative lifetimes for monolayer TMDs with experiments with a focus on monolayer MoS$_2$. At low temperature for MoS$_2$, we find excellent agreement with available experiments, as discussed next. Korn et al.[21] measured the time-resolved PL in monolayer MoS$_2$ excited with 3 eV light. At 4 K, our computed radiative lifetime of 3.7 ps is in very good agreement with their PL decay time of ∼5 ps. While they hypothesized that at such short time scale the initially generated excitons may not be thermalized, recent measurements with femtosecond resolution showed that thermalization for ∼3 eV

excitation occurs in less than 1 ps.[18] For this reason, the signal observed in ref 21 can be attributed to the intrinsic radiative decay time of the A exciton at 4 K. This is confirmed by the work from Lagarde et al.,[22] who recently measured the time-resolved PL of monolayer MoS$_2$ excited resonantly at the A exciton and observed a PL decay time of 4.5 ps, in excellent agreement with our computed value.

As the temperature is increased, time-resolved PL experiments on MoS$_2$ show the appearance of a longer PL decay time,[21] although the ∼5 ps component also present at low temperature dominates PL decay.[21,22] Room-temperature transient absorption experiments by Shi et al.[18] on suspended monolayer MoS$_2$ show a triexponential decay signal with time constants of 2 ps, 75 ps, and 0.85 ns. They tentatively attribute the 2 ps time to exciton trapping at defects, the 75 ps to hot carrier thermalization, and the 0.85 ns to radiative A exciton recombination.[18] We obtain an effective radiative lifetime of 0.82 ns at room temperature, which is in excellent agreement with the 0.85 ns decay signal observed experimentally. This result indicates that the room-temperature radiative lifetime is of order 1 ns at room temperature and corresponds to the longer PL decay component observed in time-resolved PL experiments.[18,21,22] Multiple factors can account for remaining discrepancies between computed and experimental radiative lifetimes, including the presence of defects, impurities, and flake edges in the experiment. In addition, while our calculations refer to ideally 2D monolayers surrounded by vacuum, experiments can be carried out on either suspended or substrate-supported monolayers, thus adding a potential source of discrepancy between theory and experiment.

On the basis of our data, we propose an explanation to the open question raised in ref 22 of whether the fast ∼5 ps decay component observed both at low temperature and room temperature in monolayer MoS$_2$ is associated with nonradiative processes or an intrinsic exciton lifetime. Our data shows that at low temperature the intrinsic lifetime of the A exciton is ∼5 ps, while at room temperature the intrinsic lifetime is ∼1 ns. The fact that the 5 ps PL decay is still present in experiments at room temperature strongly suggests that this characteristic lifetime is related to exciton trapping at defects resulting in PL.[22] Because at room temperature this trapping process is much faster than the time scale for radiative recombination, two characteristic recombination times are observed. On the other hand, at low temperature the intrinsic and defect-induced

recombinations occur on the same time scale of 5 ps and cannot be distinguished experimentally.

The radiative lifetimes for the other monolayers studied here are also in the range of 2−5 ps at 4 K and 1−5 ns at room temperature (see Table 1). In cases where experiments are available, our computed lifetimes are within ∼10−20% of the measured values. This provides confidence in our results for cases where experiments are not available. We find that at low temperature the radiative lifetimes in Mo-based monolayers are ∼1.5 times longer than those in W-based monolayers with the same chalcogen atom, while at room temperature the W-based monolayers exhibit ∼5 times longer effective lifetimes. The latter trend is due to the larger spin−orbit splitting in the W-based than in the Mo-based monolayers, leading to a higher weight of the dark states in the thermal average in eq 4, and thus to longer effective lifetimes. We suggest that these trends may extend to other TMDs beyond those studied here.

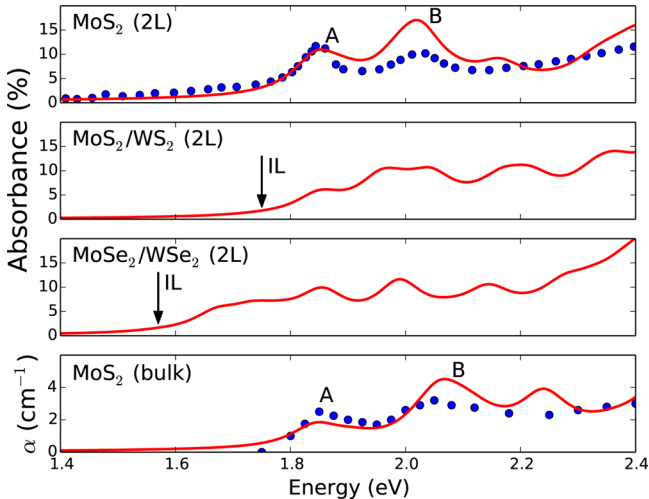Next, we discuss the absorption (Figure 3) and radiative lifetimes (Figure 4 and Table 2) in bilayer and bulk MoS_2, and

Figure 3. BSE (red line) and experimental (blue dots) absorption spectra of MoS_2 bilayer and bulk and the MoS_2/WS_2 and $MoSe_2/WSe_2$ heterobilayers. For the bulk, absorption is expressed in cm^{-1} units, and for the bilayers in percent absorbance units. The experimental data are taken from ref 12 and ref 42 for bilayer and bulk MoS_2, respectively. The labels for MoS_2 indicate the peaks associated with the A and B excitons, and the arrows for the heterobilayers indicate the interlayer (IL) excitons. The computed spectra for bilayer and bulk MoS_2 were red-shifted by ∼150 meV to match the experimental absorption onsets, while no shifts were applied to the spectra of the heterobilayers.

in the MoS_2/WS_2 and $MoSe_2/WSe_2$ heterobilayers with AB stacking[9] in the vertical direction. We find that for bilayer MoS_2 the absorbance is twice the value of monolayer MoS_2, as observed experimentally.[12] In contrast, the absorbance value in the heterobilayers deviates from the sum of the values in the two composing monolayers; we also observe the appearance of an absorption peak associated with an interlayer exciton with energy lower than the absorption onsets of the isolated monolayers.

Two main results emerge from our study of the radiative lifetimes in bilayer and bulk TMDs. First, bilayer and bulk MoS_2 show significantly higher radiative lifetimes than the monolayer case. Although bilayer and bulk MoS_2 are indirect gap materials, the direct gap at **K** determines the optical
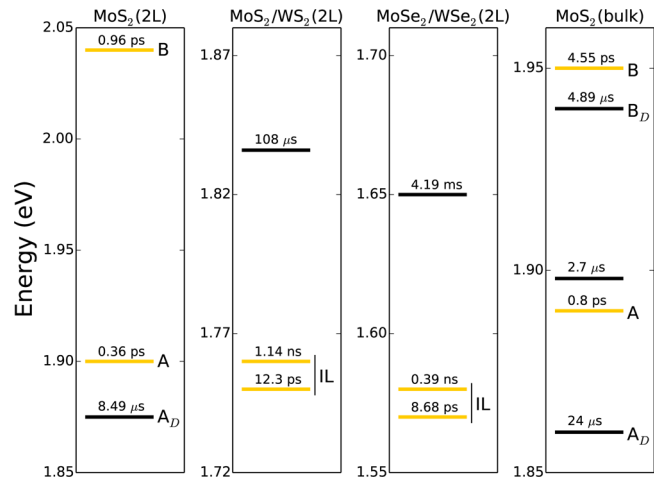

Figure 4. Energy and intrinsic radiative lifetimes $\tau_S(0)$ at 0 K for the lowest-energy excitons in MoS_2 bilayer and bulk and in the MoS_2/WS_2 and $MoSe_2/WSe_2$ heterobilayers. The dark and bright excitons are shown with black and yellow lines, respectively. The labels for MoS_2 indicate the A and B excitons, and dark states are labeled with a D subscript. The labels for the heterobilayers indicate the interlayer (IL) excitons.

Table 2. Radiative Lifetimes in Bilayer and Bulk TMDs[a]

		MoS_2 (2L)	$MoS_2/$ WS_2 (2L)	$MoSe_2/WSe_2$ (2L)	MoS_2 (bulk)
E	(eV)	1.9	1.75	1.57	1.9
$\tau(0)$	(ps)	0.36	12.3	8.7	0.8
$\langle\tau^{LT}\rangle$	(ps)	5.9	205	175 (900 at 20 K)	9
τ_{exp}^{LT}	(ps)			(1800 at 20 K) (S)	
$\langle\tau^{RT}\rangle$	(ns)	0.44	15	12.8	0.69
$\langle\tau_{eff}^{RT}\rangle$	(ns)	1.3	29.6	21	2.7
τ_{exp}^{RT}	(ns)	0.71[18] (s)			>2.6[18] (S)

[a]The data refers to the lowest-energy bright exciton. E is the exciton energy, and $\tau(0)$ the radiative lifetime at 0 K. $\langle\tau^{LT}\rangle$ and $\langle\tau^{RT}\rangle$ are the computed radiative lifetimes at low temperature (4 K) and room temperature, respectively, and τ_{exp}^{LT} and τ_{exp}^{RT} are the corresponding experimental values. For the $MoSe_2/WSe_2$ hetero-bilayer, the lifetimes at 20 K are also shown. $\langle\tau_{eff}^{RT}\rangle$ is the room temperature effective lifetime (see eq 4). In the experimental data, (s) indicates a suspended layer, and (S) indicates a substrate-supported layer.

absorption onset and main PL peaks.[12] Following photo-excitation above the direct gap at **K**, excitons can either relax to the indirect-gap CBM and VBM occurring at different points of the BZ,[43] or alternatively thermalize at **K** and emit hot photoluminescence by radiative recombination of the A exciton.[12] These two processes compete on a similar time scale and can both be observed depending on the experimental conditions.[12,18,43] Our calculations for bilayer and bulk MoS_2 yield lowest-energy bright excitons contributed by electron and hole states at **K**; these excitons are thus equivalent to the A exciton in monolayer MoS_2. Our computed room-temperature radiative lifetime for the bright A exciton in bilayer MoS_2 is 440 ps, while the effective lifetime is 1.3 ns when the radiative rates of the dark and bright A excitons are thermally averaged (see Table 2). The 440 ps radiative lifetime is in reasonable agreement with the 710 ps decay signal observed in transient absorption experiments on a suspended MoS_2 bilayer.[18] This supports the interpretation in ref 18 attributing the 710 ps

decay time to the A exciton radiative recombination. The fact that the experimental lifetime is closer to the intrinsic lifetime of the bright A exciton than the effective lifetime obtained by averaging over the dark and bright excitons deserves further investigation. While it is plausible that the dark and bright excitons were not in thermal equilibrium in the experiment, it is unclear what the conditions are for dark and bright exciton to achieve thermal equilibrium in TMD systems. It is also unclear why the lifetime in the bilayer in ref 18 is shorter than in the monolayer, given that a progressive exciton delocalization over multiple layers is expected to continuously increase the lifetime from monolayer to bulk. Our data demonstrates that radiative recombination is ~2 times slower in bilayer than in monolayer MoS_2, a finding we attribute to the delocalization of the A exciton over two layers leading to lower dipole matrix elements and thus a higher radiative lifetime in the bilayer.

In bulk MoS_2, we predict a room temperature effective radiative lifetime of 2.7 ns, which is in excellent agreement with the decay time longer than 2.6 ns measured for bulk MoS_2 in ref 18. While in ref 18 the observed signal was tentatively attributed to intervalley scattering of the A exciton, we believe the signal is associated with the radiative lifetime of the A exciton given the ~3 ns time scale consistent with our calculation. Radiative recombination of the lowest-energy bright exciton is slower in the bulk than in monolayer MoS_2. We attribute this effect to the increasing delocalization of the A exciton in the layer-normal direction and believe the ~3 ns time scale found here for the bulk constitutes an upper limit for the radiative lifetime in multilayer MoS_2. Our calculations can explain the experimental observation that the quantum yield decreases with increasing number of layers in MoS_2.[12] Given that nonradiative processes compete with radiative recombination and quench the PL, the increasing radiative recombination lifetimes found here for increasing number of layers is consistent with the lower quantum yield for increasing thickness observed experimentally. The decrease in quantum yield as a function of layer number has been observed in other TMDs, and we suggest it is a general trend due to the delocalization of the A exciton together with the competing nonradiative recombination induced by the indirect gap in the multilayers.

The second point emerging from our study of multilayer TMDs is the dramatic increase in the radiative lifetimes in the MoS_2/WS_2 and $MoSe_2/WSe_2$ heterobilayers. We predict that in both systems the lowest-energy exciton has interlayer character,[44,45] that is, it is constituted by an electron localized on one layer and a hole on the other layer composing the bilayer heterojunction. In the cases studied here, upon formation of a heterojunction between the Mo- and W-based monolayers (with the same chalcogen atom) a type-II band alignment is achieved due to the different band gaps and electron affinities in the composing monolayers.[8] At the interface, the CBM originates from states in the Mo-based monolayer and the VBM from states in the W-based monolayer. The spatial separation of the electron and hole becomes apparent by plotting the exciton wave function (see Figure 5). When the position of the hole is fixed on the W-based monolayer, the electronic charge density localizes on the Mo-based monolayer, thus confirming the interlayer character of the exciton.

The reduced spatial overlap between the electron and the hole decreases the transition matrix element and results in longer radiative lifetimes, while at the same time the bright
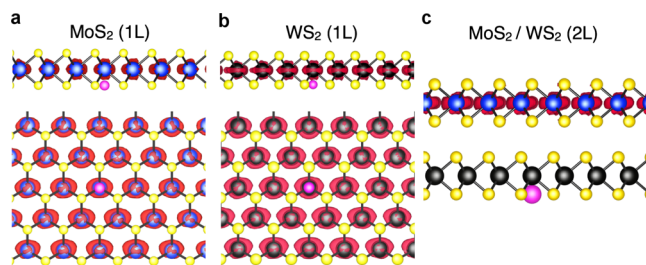

Figure 5. Side view (top panel) and top view (bottom panel) of exciton charge densities in (a) monolayer MoS_2, (b) monolayer WS_2 (a), and (c) the MoS_2/WS_2 heterobilayer (side view only). Shown is the electronic charge density (in red) when the hole is set in a fixed position (shown with a pink sphere). In the monolayers in (a) and (b), the electronic charge spreads over the entire layer due to the delocalized nature of the exciton. In the heterobilayer, when the hole is fixed in the WS_2 layer, the electron spreads over the MoS_2 layer due to the interlayer character of the exciton. The atoms are shown as blue (Mo), black (W), and yellow (S) spheres.

character of the exciton is preserved. We predict effective room temperature lifetimes for these long-lived excitons of ~30 ns in MoS_2/WS_2 and 21 ns in $MoSe_2/WSe_2$. A very recent experimental observation of long-lived interlayer excitons in $MoSe_2/WSe_2$ has shown a measured radiative lifetime of 1.8 ns at 20 K (see ref 44). For comparison, our computed lifetime at 20 K for the same system is 0.9 ns and thus within a factor of 2 of the experimental value. While this result confirms the long-lived character of the interlayer excitons observed experimentally, better agreement with experiment may be achieved using a more realistic bilayer structure including nonideal AB stacking between the two layers.

The measurements in ref 44 further show the presence of two low-energy interlayer excitons,[44] which is in agreement with the two interlayer bright excitons obtained in our calculations (see Figure 4). Interlayer excitons attributed to type-II band alignment have recently been observed experimentally also in MoS_2/WS_2,[45] consistent with our results. Reference 45 further shows that interlayer excitons are present regardless of the stacking geometry of the two layers in the vertical direction; we thus expect that long-lived excitons in heterobilayers are not limited to the AB-stacking geometry studied here. These results further confirm that our approach yields highly accurate exciton character and lifetimes in multilayer TMDs.

The tunability of the radiative lifetimes over several orders of magnitude with number of layers, stacking sequence, and temperature enables unprecedented control of exciton dynamics in 2D-TMDs. The ability to control exciton dynamics plays a key role in optoelectronic and renewable energy technologies. In photovoltaics, long-lived excitons are necessary to guarantee electron−hole dissociation before exciton recombination, and the radiative quantum yield is linked to the power conversion efficiency. In addition, TMD heterostructures may enable fabrication of multijunction solar cells free of epitaxial strain in which light absorption and exciton dynamics are controlled within each stacked monolayer. As the edges of TMD flakes can reduce water to hydrogen in photocatalytic cells,[5,6] studies of exciton dynamics can provide valuable information to understand reaction kinetics. Tunable PL frequency and radiative lifetimes further hold unique potential for the development of novel light-emitting diodes and lasers based on TMDs.[7] Finally, there is rising evidence

that trion excitations are involved in the excited state dynamics in 2D-TMDs. We believe trions deserve further investigation using ab initio methods. This will likely require treatments involving the three-particle Green's function and thus beyond the *GW*-BSE formalism.

In conclusion, we develop and use first-principles calculations of radiative lifetimes in layered 2D-TMDs. Our results provide crucial microscopic insight to interpret time-resolved experiments. The ability to predict accurate exciton energies and radiative lifetimes shown here will be of key importance to understand excited state dynamics and energy conversion mechanisms in the next generation of TMD based devices.

Methods. *Computational Methods.* We carry out DFT calculations within the local-density approximation (LDA) using the Quantum Espresso package.[31] The TMD structures are prepared using the experimental lattice parameters and then relaxed within DFT, following a procedure similar to our recent work.[8] We employ fully relativistic pseudopotentials and treat the *sp* semicore states of the transition metal atoms as valence electrons.[8,16] The quasiparticle bandstructures are computed using the *GW* approach as implemented in the Yambo code.[32] We employ the "one-shot" G_0W_0 approximation,[26] a plasmon-pole model for the dielectric function in the *GW* self-energy, cutoff energies of 60 and 10 Ry for the exchange and correlation parts of the *GW* self-energy, respectively, and up to 300 empty bands. We use a $27 \times 27 \times 1$ **k**-point grid for the monolayers, a $18 \times 18 \times 1$ **k**-point grid for the bilayers, and a $18 \times 18 \times 2$ **k**-point grid for the bulk TMDs. The Coulomb interaction is truncated in the layer-normal direction to avoid spurious interactions with the image systems. We employ the BSE to compute the optical spectra in Figure 1 and Figure 3, using the same **k**-point grids employed in the *GW* calculations and including six valence and six conduction states in the excitonic Hamiltonian. Our approach takes fully into account the spinorial nature of the electronic Kohn–Sham states in the *GW* and BSE calculations.

■ ASSOCIATED CONTENT

Ⓢ Supporting Information
GW bandstructures of MoS$_2$, WS$_2$, MoSe$_2$, and WSe$_2$. Detailed derivation of eqs 1–3. This material is available free of charge via the Internet at http://pubs.acs.org.

■ AUTHOR INFORMATION

Corresponding Author
*E-mail: jcg@mit.edu.

Author Contributions
M.P. and M.B. contributed equally to this work.

Notes
The authors declare no competing financial interest.

■ ACKNOWLEDGMENTS

■ REFERENCES

(1) Radisavljevic, B.; Radenovic, A.; Brivio, J.; Giacometti, V.; Kis, A. *Nat. Nanotechnol.* **2011**, *6*, 147–150.

(2) Novoselov, K. S.; Jiang, D.; Schedin, F.; Booth, T. J.; Khotkevich, V. V.; Morozov, S. V.; Geim, A. K. *Proc. Natl. Acad. Sci. U.S.A.* **2005**, *102*, 10451–10453.

(3) Britnell, L.; Ribeiro, R. M.; Eckmann, A.; Jalil, R.; Belle, B. D.; Mishchenko, A.; Kim, Y.-J.; Gorbachev, R. V.; Georgiou, T.; Morozov, S. V.; Grigorenko, A. N.; Geim, A. K.; Casiraghi, C.; Neto, A. H. C.; Novoselov, K. S. *Science* **2013**, *340*, 1311–1314.

(4) Wang, H.; Yu, L.; Lee, Y.-H.; Shi, Y.; Hsu, A.; Chin, M. L.; Li, L.-J.; Dubey, M.; Kong, J.; Palacios, T. *Nano Lett.* **2012**, *81*, 109–162.

(5) Jaramillo, T. F.; Jørgensen, K. P.; Bonde, J.; Nielsen, J. H.; Horch, S.; Chorkendorff, I. *Science* **2007**, *317*, 100–102.

(6) Kibsgaard, J.; Chen, Z.; Reinecke, B. N.; Jaramillo, T. F. *Nat. Mater.* **2012**, *11*, 963–969.

(7) Eda, G.; Maier, S. A. *ACS Nano* **2013**, *7*, 5660–5665.

(8) Bernardi, M.; Palummo, M.; Grossman, J. C. *Nano Lett.* **2013**, *13*, 3664–3670.

(9) Chhowalla, M.; Shin, H. S.; Eda, G.; Li, L. J.; Loh, K. P.; Zhang, H. *Nat. Chem.* **2013**, *5*, 263–275.

(10) Ataca, C.; Sahin, H.; Ciraci, S. *J. Phys. Chem. C* **2012**, *116*, 8983–8999.

(11) Splendiani, A.; Sun, L.; Zhang, Y.; Li, T.; Kim, J.; Chim, C. Y.; Galli, G.; Wang, F. *Nano Lett.* **2010**, *10*, 1271–1275.

(12) Mak, K.; Lee, C.; Hone, J.; Shan, J.; Heinz, T. *Phys. Rev. Lett.* **2010**, *105*, 136805.

(13) Mak, K. F.; He, K.; Shan, J.; Heinz, T. F. *Nat. Nanotechnol.* **2012**, *7*, 494–498.

(14) Xiao, D.; Liu, G.-B.; Fenf, W.; Xu, X.; Yao, W. *Phys. Rev. Lett.* **2012**, *108*, 196802.

(15) Qiu, D.; Da Jornada, G.; Louie, S. *Phys. Rev. Lett.* **2013**, *111*, 216805.

(16) Cheiwchanchamnangij, T.; Lambrecht, W. R. L. *Phys. Rev. B* **2012**, *85*, 205302.

(17) Cao, T.; Wang, G.; Han, W.; Ye, H.; Zhu, C.; Shi, J.; Niu, Q.; Tan, P.; Wang, E.; Liu, B.; Feng, J. *Nat. Commun.* **2012**, *3*, 887.

(18) Shi, H.; Yan, R.; Bertolazzi, S.; Brivio, J.; Gao, B.; Kis, A.; Jena, D.; Xing, H. G.; Huang, L. *ACS Nano* **2013**, *7*, 1072–1080.

(19) Cui, Q.; Ceballos, F.; Kumar, N.; Zhao, H. *ACS Nano* **2014**, *8*, 2970–2976.

(20) Peimyoo, N.; Shang, J.; Cong, C.; Shen, Z.; Wu, X.; Yeow, E. K. L.; Ting, Y. *ACS Nano* **2013**, *7*, 10985–10994.

(21) Korn, T.; Heydrich, S.; Hirmer, M.; Schmutzler, J.; Schüller, C. *Appl. Phys. Lett.* **2011**, *99*, 102109.

(22) Lagarde, D.; Bouet, L.; Marie, X.; Zhu, C. R.; Liu, B. L.; Amand, T.; Tan, P. H.; Urbaszek, B. *Phys. Rev. Lett.* **2014**, *112*, 047401.

(23) Sim, S.; Park, J.; Song, J.-G.; In, C.; Lee, Y.-S.; Kim, H.; Choi, H. *Phys. Rev. B* **2013**, *88*, 075434.

(24) Kozawa, D., Kumar, R., Carvalho, A., Amara, K. K., Zhao, W., Wang, S., Toh, M., Ribeiro, R. M., Neto, A. C., Matsuda, K., Eda, G. *Nat. Commun.* **2014**5.

(25) Martin, R. *Electronic Structrure: Basic Theory and Practical Methods*; Cambridge University Press: New York, 2008.

(26) Onida, G.; Reining, L.; Rubio, A. *Rev. Mod. Phys.* **2002**, *74*, 601–659.

(27) Hybertsen, M. S.; Louie, S. G. *Phys. Rev. B* **1986**, *34*, 5390–5413.

(28) Bernardi, M.; Vigil-Fowler, D.; Lischner, J.; Neaton, J. B.; Louie, S. G. *Phys. Rev. Lett.* **2014**, *112*, 257402.

(29) Rozzi, C. A.; Falke, S. M.; Spallanzani, N.; Rubio, A.; Molinari, E.; Brida, D.; Maiuri, M.; Cerullo, G.; Schramm, H.; Christoffers, J.; Christoph, L. *Nat. Commun.* **2013**, *4*, 1602.

(30) Falke, S. M.; Rozzi, C. A.; Brida, D.; Maiuri, M.; Amato, M.; Sommer, E.; de Sio, A.; Rubio, A.; Cerullo, G.; Molinari, E.; Lienau, C.; et al. *Science* **2014**, *344*, 1001–1005.

(31) Giannozzi, P. *J. Phys.: Condens. Matter* **2009**, *21*, 395502.

(32) Marini, A.; Hogan, C.; Gruning, M.; Varsano, D. *Comput. Phys. Commun.* **2009**, *180*, 1392–1403.

(33) Spataru, C.; Ismail-Beigi, S.; Capaz, R.; L, S. G. *Phys. Rev. Lett.* **2005**, *95*, 247402.

(34) Andreani, L. *Solid State Commun.* **1991**, *77*, 641–645.

(35) Citrin, D. *Solid State Commun.* **1992**, *84*, 281−284.

(36) Perebeinos, V.; Tersoff, J.; Avouris, P. *Nano Lett.* **2005**, *5*, 2495−2499.

(37) Ramasubramaniam, A. *Phys. Rev. B* **2012**, *86*, 115409.

(38) Ye, Z.; Cao, T.; O'Brien, K.; Zhu, H.; Yin, X.; Wang, Y.; Louie, S. G.; Zhang, X. *Nature* **2014**, *513*, 214−218.

(39) Wang, G.; Bouet, L.; Lagarde, D.; Vidal, M.; Balocchi, A.; Amand, T.; Marie, X.; Urbaszek, B.*Phys. Rev. B* **2014**, *90*, 075413.

(40) Kumar, N.; Cui, Q.; Ceballos, F.; He, D.; Wang, Y.; Zhao, H. *Phys. Rev. B* **2014**, *89*, 125427.

(41) Shinichiro, M.; Yuhei, M.; Minglin, T.; Weijie, Z.; Goki, E.; Kazunari, M. *Phys. Rev. B* **2014**, *90*, 155449.

(42) Beal, A.; Hughes, H. *J. Phys. C.: Solid State Phys.* **1979**, *12*, 881−890.

(43) Kumar, N.; He, J.; He, D.; Wang, Y.; Zhao, H. *J. Appl. Phys.* **2013**, *113*, 133702.

(44) Rivera, P.; Schaibley, J. R.; Jones, A. M.; Ross, J. S.; Wu, S.; Aivazian, G.; Klement, P.; Ghimire, N. J.; Yan, J.; Mandrus, D. G.; Yao, W.; Xu, X. *Nat. Commun.* **2015**, *6*, 6242.

(45) Yu, Y.; Hu, S.; Su, L.; Huang, L.; Liu, Y.; Jin, Z.; Purezky, A. A.; Geohegan, D. B.; Kim, K. W.; Zhang, Y.; Cao, L. *Nano Lett.* **2015**, *15*, 486−491.